CRC Report No. AVFL-32

Phase 1

EFFECTS OF KNOCK INTENSITY MEASUREMENT TECHNIQUE AND FUEL CHEMICAL COMPOSITION ON THE RESEARCH OCTANE NUMBER (RON) OF FACE GASOLINES: PART 2 - EFFECTS OF SPARK TIMING

February 2023

COORDINATING RESEARCH COUNCIL, INC.

5755 NORTH POINT PARKWAY • SUITE 265 • ALPHARETTA, GA 30022

The Coordinating Research Council, Inc. (CRC) is a non-profit corporation supported by the petroleum and automotive equipment industries. CRC operates through the committees made up of technical experts from industry and government who voluntarily participate. The four main areas of research within CRC are: air pollution (atmospheric and engineering studies); aviation fuels, lubricants, and equipment performance; heavy-duty vehicle fuels, lubricants, and equipment performance (e.g., diesel trucks); and light-duty vehicle fuels, lubricants, and equipment performance (e.g., passenger cars). CRC's function is to provide the mechanism for joint research conducted by the two industries that will help in determining the optimum combination of petroleum products and automotive equipment. CRC's work is limited to research that is mutually beneficial to the two industries involved. The final results of the research conducted by, or under the auspices of, CRC are available to the public.

JOURNAL PUBLICATION REFERENCE

This version of the manuscript was reviewed by the AVFL committee prior to submission to the Journal of Fuel for review. The final version published by the Journal of Fuel, "Effects of Knock Intensity Measurement Technique and Fuel Chemical Composition on the Research Octane Number (RON) of FACE Gasolines: Part 2 – Effects of Spark Timing," can be downloaded at:
https://doi.org/10.1016/j.fuel.2023.127694

Effects of Knock Intensity Measurement Technique and Fuel Chemical Composition on the Research Octane Number (RON) of FACE Gasolines: Part 2 – Effects of Spark Timing

Alexander Hoth, Christopher P. Kolodziej

Argonne National Laboratory, 9700 S. Cass Avenue, Lemont, IL 60439, USA

Keywords: RON, Knock-limited spark advance, Lambda effects, Knock characterization

Abstract

The Research and Motor Octane Number (RON, MON) characterize a fuel's knock resistance by rating the knock intensity of a sample fuel relative to that of Primary Reference Fuels (PRF) in a Cooperative Fuel Research (CFR) Engine. A fuel's octane number is regulated to prevent damage from autoignition leading to knocking combustion in spark-ignition engines. The operational differences between the standard RON rating and modern engine operation are explored in a three-part publication series. The previous study focused on the effects of lambda and knock characterization. This second study primarily focuses on the effects of spark timing on RON determination. Following the findings from the first publication, the knock intensity was captured by the knockmeter and by the maximum amplitude of pressure oscillations (MAPO) at the lambda of peak knock intensity and stoichiometry. Knock-limited spark advance tests were conducted for a set of seven Fuels for Advanced Combustion Engines (FACE) from the Coordinating

Research Council (CRC) with varying chemical composition, PRFs, and Toluene Standardization Fuels (TSFs). For retarded spark timings, pre-spark low-temperature heat release was found for low RON PRFs. Low RON PRFs also showed knocking characteristics before reaching the center of combustion suggesting that the use of knock-limited spark advance (KLSA) was preferred over the knock-limited combustion phasing. Primarily paraffinic fuels tended towards increased pressure oscillations while dominantly aromatic fuels experienced higher pressure rise rates. A MAPO-based KLSA correlated best to Octane Index at a negative K-factor suggesting beyond RON operation despite being at otherwise RON conditions. At stoichiometry, the MAPO-based KLSA did neither correlate to RON nor Octane Index. Good agreement was found between KLSA-based effective RON from this study to the MAPO-based effective RON from the first study.

1. Introduction

Modern engines push towards higher engine efficiency through means of an increased compression ratio and downsizing in combination with boosting. Those technologies increase pressure and temperature in the combustion chamber of spark-ignition engines, which can lead to an undesired cascading autoignition and subsequently potentially harmful high-frequency pressure oscillations called knock [1]. The research (RON) and motor octane number (MON) are fuel properties that characterize the fuel's resistance to autoignition [2, 3]. However, the assessment of RON and MON compared to the knock-limited operation of modern commercial engines differ significantly as outlined in *Table 1*.

RON and MON rate the knock intensity of a sample fuel relative to the knock intensity of two bracketing primary reference fuels (PRF) [2]. However, the knock intensity is assessed with a knockmeter system which attenuates high-frequency pressure oscillations as outlined by multiple studies [4 - 7]. On the other hand, modern research engines limit the maximum amplitude of pressure oscillations (MAPO) during operation [4, 6, 8, 9]. For this study, MAPO is calculated as the peak value of a band-pass filtered (4 – 18 kHz) and rectified cylinder pressure signal. More details about the calculation of MAPO can be found in the previous publication [4]

The octane numbers of the fuels are assessed at the lambda of the highest knock intensity which equals the worst performance of the fuel. The first study of this three-part publication series and a previous study by the authors found the lambda of peak knock intensity, both knockmeter- and MAPO-based, to occur at fuel-rich conditions. Ethanol as well as olefins and cycloparaffins shifted the lambda of peak knock closer toward stoichiometry [4, 10, 11]. The value of lambda at peak MAPO and peak knockmeter occurs typically within close proximity of each other [4, 12].

The octane numbers are rated on the Cooperative Fuel Research (CFR) engine which has a variable compression ratio adjustable to the respective octane number of the sample fuel while in operation.

Modern research engines typically have a fixed, but interchangeable compression ratio. Due to the fixed compression ratio, modern engines have to retard the spark timing to limit knocking combustion at high load operating conditions. The knock-limited combustion phasing (KLCA50) and the knock-limited spark advance (KLSA) are typical ways to identify the knock limit of a modern research engine at a given pressure-based MAPO knock intensity threshold [9, 13]. During RON rating, the CFR engine has a fixed spark timing at 13°bTDC (-13°aTDC) and rates the variable knockmeter-based knock intensity [2]. This is opposing the variable spark timing operation for maintaining a fixed MAPO-based knock intensity threshold in modern SI engines.

Table 1. Overview of the discrepancy in operating conditions between the RON rating procedure and knock-limited spark advance type testing utilized in modern commercial engines.

Parameter	**RON Rating [2]**	**KLSA type testing**
Knock Intensity	CFR knockmeter system	Cylinder pressure oscillations
Lambda	Peak knockmeter reading	Generally stoichiometric
Spark Timing	Constant at 13°bTDC (-13°aTDC)	Limited by incipient knock
Compression Ratio	Variable, depending on RON	Fixed / Interchangeable

The differences in the rating methodology between the RON assessment and modern engine operation lead to discrepancies between the RON of a gasoline and its actual knock limiting quality in modern engines [6, 8, 12, 13]. Other operating conditions, such as the slow CFR engine speed of 600 rpm and the side-mounted spark plug in the CFR engine can contribute to the reported discrepancy as well. Yates et al. showed the pressure-temperature trajectories of standard RON and MON tests and the impact of modern engine technologies such as direct injection and turbocharging. This shifted the pressure-temperature trajectory towards higher pressures into the beyond RON region [14]. Kalghatgi proposed

the Octane Index (OI) which uses an engine operation-specific weighting factor K to interpolate or extrapolate between the RON and MON trajectory, equation 1. The RON trajectory represents a K-factor of K = 0 while MON is represented when K = 1 [15, 16]. Mittal et al. showed, that historically, in the 1950s, K-factors between 0 and 1 were representative of engine performance. Modern engine operation as of 2009 resulted in a range of K = -0.6 to 0.2 [17]. A negative K-factor leads to a higher Octane Index with increased RON-MON sensitivity and therefore higher knock resistance for lower MON values for a fuel with a given RON [13, 17].

$$OI = RON - K * (RON - MON) \quad \text{(Equ. 1) [15]}$$

The combustion phasing plays a critical role in engine efficiency and knock prevention. The RON test utilizes a constant spark timing which leads to a variation of the center of combustion solely due to differences in the laminar flame speed of the fuel. The center of combustion is identified as the crank angle of 50% mass fraction burned (CA50). Ethanol was previously found to slightly advance the combustion phasing during flame propagation [10, 18].

Hauber et al. proposed a novel gasoline knock index, which utilized a variable spark timing to maintain a constant CA50 [11]. Other updates include rating the knock intensity of fuels based on pressure oscillations and operating the CFR engine at stoichiometry [11]. The rating methodology showed good agreement between the gasoline knock index and RON but did not address the discrepancy between RON and knock limited combustion phasings in modern engines.

Multiple studies from Syzbist et al, Pulpeiro Gonzalez et al., and Vuilleumier et al. showed KLSA type testing for the Co-Optima core fuels in SI modern engines [13, 19, 20]. These fuels are blended to a constant RON of 98 while changing the chemical composition from highly paraffinic to highly aromatic and also include a RON 98 fuel with 30 vol% ethanol. While at a constant RON of 98, those fuels significantly varied in their KLCA50 as summarized in a previous study by the authors [12].

Low-temperature heat release is typically seen during homogenous charge compression ignition but a recent study by the authors found that low-temperature chemistry also occurs during spark ignition combustion while being covered up by the main heat release from the propagating flame [21]. A significant retard in spark timing could visualize such pre-spark low-temperature chemistry.

The first part of this three-part publication series explored the effects of switching from a knockmeter-based knock intensity assessment to a MAPO-based knock threshold as well as switching from the lambda of peak knock intensity to stoichiometry (rows one and two from *Table 1*). The knockmeter system was found to filter out high-frequency signal components typically associated with knocking combustion. Despite the differences in knock measurement principle, the lambda of peak knockmeter and lambda of peak MAPO closely matched. Based on a MAPO knock threshold of 0.1 bar, all cycles for the CRC fuels were knocking during standard RON testing. Significant offsets between the standard RON rating and the MAPO-knock intensities at standard RON operation were found. The best correlation between the MAPO knock intensity under standard RON conditions and Octane Index was found for K = -0.48 which would represent standard RON operation but using a MAPO-based knock intensity [4].

This study rated the seven CRC FACE fuels via a knock-limited spark advance (KLSA) test similar to modern engine knock characterization (row three of *Table 1*). The tests were performed at stoichiometry as well as at the lambda of the highest knock intensity following the findings from the first paper. Both the knockmeter-based and the MAPO-based knock intensity of the sample fuels were rated relative to PRFs to calculate an equivalent RON based on the fuel's KLSA. A comparison to the standard RON ratings of the fuels showed vastly different levels of correlation to standard RON depending on the type of knock intensity measurement technique as well as the applicable lambda. Further, a comparison to the effective MAPO-based RON calculations from the first paper was explored.

2. Experimental Procedures

For this experimental study, a single-cylinder, variable compression ratio, naturally aspirated, and carbureted CFR F1 engine was used. This represents the standard octane rating engine for RON conditions according to ASTM D2699. The engine was upgraded to encompass modern research engine measurement equipment, such as an indicated cylinder pressure measurement via a measuring spark plug and a wide-band lambda sensor. In addition, the spark timing was monitored using a current clamp. More details about the used sensors and a full list of installed measurement devices are included in *Table 5* in the appendix and listed in the first part of this publication series [4]. It is important to note, that no changes to the geometry of intake, cylinder, or exhaust were made to retain the engine compliance with the ASTM D2699 method [2].

Seven fuels for advanced combustion engines (FACE) from the Coordinating Research Council (CRC) were tested in this study. *Table 2* summarizes the octane numbers, the 90% evaporation temperature, and the composition of each FACE gasoline. Based on their composition, the FACE fuels were characterized as mainly paraffinic or mainly aromatic fuels. Each of the two groups also includes gasolines that have olefins, cycloparaffins or 15 vol% ethanol added. Additional details are included in previous CRC reports and the first part of this publication series [4, 22]. Both this study and the previous study compare the seven FACE fuels to numerous bracketing PRFs and two applicable toluene standardization fuels (TSFs) as specified in the ASTM D2699 method.

Table 2. Fuel overview with physical properties and chemical composition.

O – Olefin, cP – Cyclo-Paraffinic, E15 – 15 vol Ethanol [22]

FACE Fuel	RON	MON	S	T90 (°F)	Iso-paraffin (vol%)	Aromatic (vol%)	N-Paraffin (vol%)	Cyclo-Paraffin (vol%)	Olefin (vol%)	Categorization	Symbol
B	95.8	92.4	3.4	236	86.9	5.8	8.0	0.1	0.02	Iso-paraffinic	
D	94.2	87.0	7.2	331	42.1	33.4	24.1	0.1	0.04	Aromatic	
F	94.0	88.1	5.9	242	67.6	7.7	4.4	11.0	9.4	Iso-paraffinic, O, cP	
G	96.5	85.8	10.7	343	38.4	33.6	6.7	11.5	8.1	Aromatic, O, cP	
A + E15	94.8	89.4	5.4	219	73.1	0.3	9.9	1.4	0.2	Iso-paraffinic, E15	
C + E15	94.8	88.8	6.0	241	59.3	3.3	20.8	0.3	1.1	Iso-paraffinic, E15	
H + E15	94.1	83.3	10.8	323	19.4	30.4	19.1	8.9	5.8	Aromatic, O, cP, E15	

Key differences between standard RON testing and modern engine knock rating were summarized in *Table 1*. For this testing, variations of the standard RON test were established to mimic the knock rating procedure of modern engines by varying the spark timing to achieve pre-defined knock intensity thresholds. The knockmeter knock intensity was limited to 40 knock units (KU) while the MAPO threshold was set to 0.6 bar for a cyclic average across 300 consecutive cycles. The 0.6 bar MAPO threshold represents a 1 bar/1000 rpm knock threshold at the RON engine speed of 600 rpm, which is a commonly used knock intensity threshold for modern engine knock calibration. *Figure 1* shows a spark timing sweep for iso-octane (PRF100) at otherwise standard RON conditions. At the standard spark timing of 13 degrees before top dead center (-13°aTDC), the MAPO knock intensity is significantly higher than the defined knock intensity threshold. When retarding the spark timing, the knock intensity dropped due to less intense pressure-temperature conditions in the cylinder. The spark timing at which the knock intensity threshold is reached is termed knock-limited spark advance (KLSA). When plotted versus the center of combustion, this is termed knock-limited crank angle of 50 % mass fraction burned (KLCA50). The mass

fraction burned was calculated using the Thermodynamics 2 function of AVL Concerto. This function calculates the apparent heat release with gamma dependent on an estimated charge temperature.

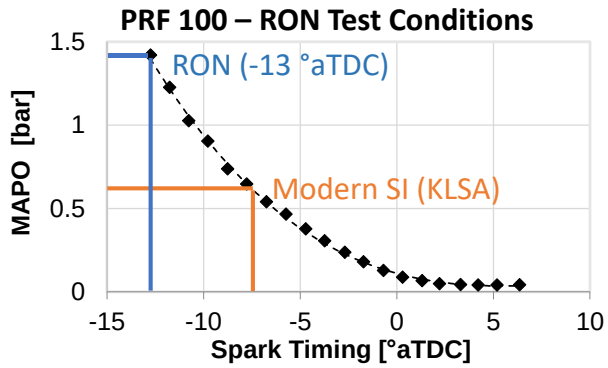

Figure 1. Pressure-based MAPO knock intensity of the standard RON test and its knock-limited spark advance (KLSA) limits

The first set of testing was performed under RON-like conditions at the lambda of highest knock intensity at the standard compression ratio for a RON 95 sample as defined by the ASTM D2699 method. Following the findings from the previous study, the second set of testing was performed at stoichiometry to better represent modern engine operation. Testing performed at stoichiometry reduced both the knockmeter and the pressure-based knock intensities [4]. To increase the knock intensities when testing at stoichiometry, an increased compression ratio was selected. Using an iterative procedure, the compression ratio and center of combustion (CA50) were varied to reach the 0.6 bar MAPO threshold and the combustion phasing of maximum gross indicated mean effective pressure (gIMEP) for FACE-G, *Figure 2*. This compression ratio was maintained for all other sample and reference fuels. FACE-G was selected since it showed the overall lowest MAPO knock intensities in the previous study [4]. Therefore, all other FACE fuels should require a retarded spark timing relative to FACE-G to limit the knock intensity.

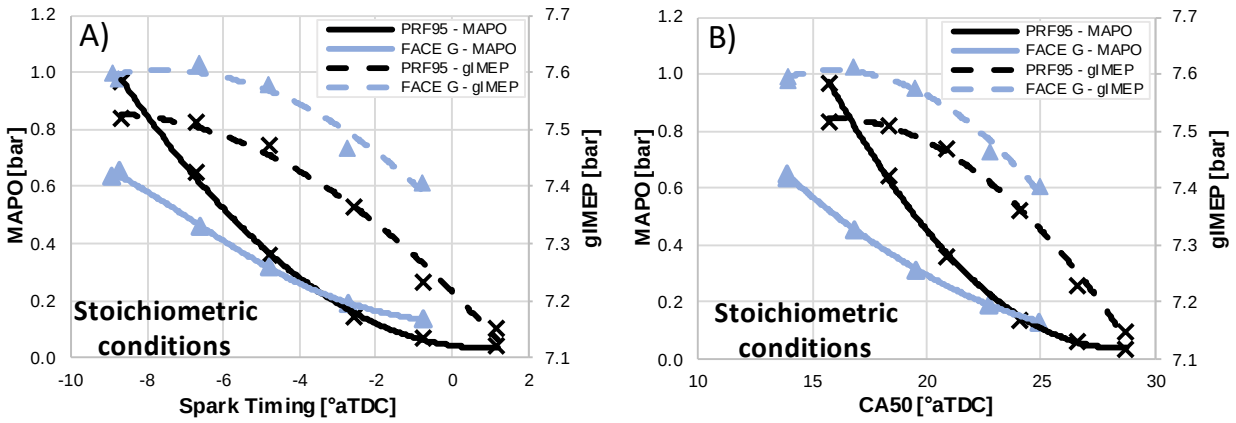

Figure 2. MAPO and the gross indicated mean effective pressure (gIMEP) as a function of spark timing and CA50.

Figure 2 shows the performed initial spark timing sweeps and the MAPO knock intensity as well as gross indicated mean effective pressure response for FACE-G and PRF95. *Figure 2A* shows the variation of the spark timing while *Figure 2B* has the same information depicted based on the center of combustion (CA50). The CA50 represents the crank angle location of 50 percent mass fraction burned. *Figure 2A* and *Figure 2B* show very similar trends of increasing knock intensities for advanced combustion phasing while gIMEP follows a parabolic shape. FACE-G has a higher gIMEP compared to PRF95. This is due to a slight advance in combustion phasing for FACE-G over PRF95 for a given spark timing. For both fuels, the maximum gIMEP occurred at a CA50 between 16 and 18 °aTDC. This is significantly later than values reported for modern engines which typically have their peak gIMEP around 8°aTDC [24]. Part of the reason is the slow engine speed of 600 rpm and the knocking combustion which constitute to increased heat transfer losses. The MAPO knock intensity of PRF95 is higher compared to MAPO of FACE-G despite a higher RON of FACE-G as found in the previous publication and listed in Table 2 [4].

As mentioned earlier, the compression ratio was set for FACE-G so that a MAPO knock intensity threshold of 0.6 bar was reached at maximum gIMEP conditions during naturally aspirated operation. The knock threshold was reached at a spark timing around -9°aTDC (CA50 of 14°aTDC). A slightly more retarded spark timing resulted in a slight increase in gIMEP, but this is of no further impact as all fuels were tested at this

particular compression ratio and the variation in gIMEP is well within the measurement uncertainty of 1.5% for the indicated spark plug [25].

3. Spark Timing Sweeps

3.1. Primary Reference Fuels

Spark timing sweeps were performed for each fuel at two lambda settings. First, at the lambda of highest knock intensity, termed peak knocking lambda, and second, at stoichiometry. At standard RON conditions, meaning peak knocking lambda, the spark timing is defined to -13°aTDC. From this starting point, the spark timing for PRFs with various RON levels was retarded until the maximum gIMEP was surpassed. As mentioned earlier, a higher compression ratio was selected for stoichiometric operation, which resulted in more retarded spark timings compared to peak knocking lambda operation. If tested at a constant compression ratio, PRFs would have an advanced spark timing for stoichiometric operation compared to operation at peak knocking lambda. The MAPO and knockmeter knock intensity response, as well as gIMEP dependence on spark timing, are presented in *Figure 3*. The previous study found significant differences in fuel performance between operation at the peak knocking lambda and stoichiometry. Therefore, left-sided plots 3A, 3C, and 3E show conditions for each fuel at its individual peak knock lambda (PKL) while right-sided plots 3B, 3D, and 3F contain experimental data at stoichiometry.

Advanced spark timings increased both the knockmeter and the MAPO knock intensities. A higher RON level resulted in lower knock intensities. Because of its high RON relative to the set compression ratio, PRF100 neither reached the knock threshold of 40 KU nor the threshold of 0.6 bar MAPO for operation at PKL. All other PRFs reached the knock intensity threshold and therefore all cycles of those fuels were knocking when taking into account the 0.1 bar MAPO threshold from the previous publication [4]. The

PRFs were reasonably linearly spaced and third-order polynomial trendlines were successfully fitted to the measurement. While not shown in the plot, each trendline had an excellent coefficient of determination ($R^2 > 0.99$). Therefore, the equation of the trendline can be used to estimate the spark timing at which the respective PRF crosses either of the knock intensity thresholds of 40 KU or 0.6 bar MAPO.

The gIMEP typically followed a parabolic shape as spark timing was modified. For PKL operation, higher RON PRFs achieved higher gIMEPs due to lower knock intensities at a given spark timing compared to lower RON PRFs. It is assumed that increased pressure oscillations penetrate the boundary layer of the combustion chamber, hence increasing the heat transfer and reducing gIMEP respectively. The PRF100 with the highest RON and therefore lowest knock intensities had the most advanced spark timing for the maximum gIMEP. At lower knock intensities at retarded spark timings, the gIMEP difference between PRFs was minimal when operated at PKL conditions. For the stoichiometric cases, a wider range of spark timings was required to account for the wider range of PRF octane levels. For spark timings after top dead center, the distribution of gIMEP was more diverse. For example, PRF87 showed an increased gIMEP at retarded spark timings compared to higher RON PRFs. This is the result of an advanced CA50 for a given spark timing as will be discussed for *Figure 4* and *Figure 5* by analyzing the two green-circled data points in *Figure 3*.

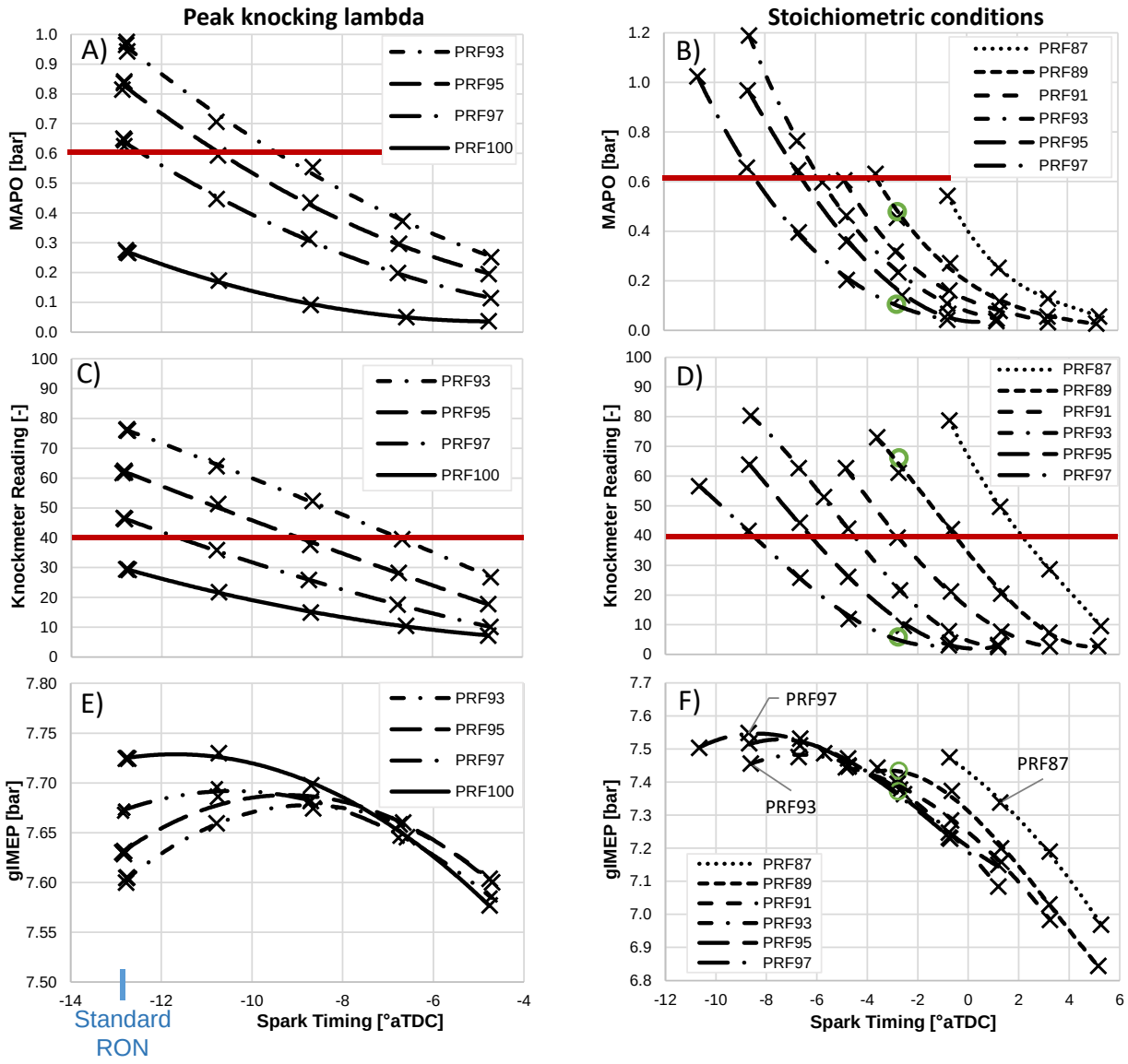

Figure 3. Spark timing sweeps at both peak knocking lambda conditions (A, C, E) and stoichiometric conditions (B, D, F) for MAPO knock intensity, knockmeter knock intensity, and gIMEP for various PRFs. The knock intensity plots show the applied knock threshold. At stoichiometric conditions, the two green-circled data points are used in Figure 5.

A common way of analyzing spark timing sweeps is to study combustion phasing (CA50). *Figure 4A* and *4B* show the MAPO and knockmeter knock intensity response versus CA50. Essentially, *Figure 3B* and *Figure 4A* depict identical measurements on a different x-axis. Plots are data point limited to depict the trendlines since an excellent correlation ($R^2 > 0.99$) between the trendline and data points was previously shown.

A cluster of PRFs (circled in blue) is shown in *Figure 4A*. At a given CA50 location (i.e. 20°aTDC), the difference of six research octane numbers between PRF87 and PRF93 caused no significant difference in the pressure-based knock intensity. This was not expected as a lower RON fuel typically showed higher knock intensities as can be seen for the knockmeter knock intensity in *Figure 4B*. The cluster of PRFs was not observed when plotting the MAPO on a spark timing basis (*Figure 3B*). The green circled data points for PRF97 and PRF89 were captured with a spark timing of -3°aTDC (compare *Figure 3B*) but differ in their CA50 location. Therefore, the change in CA50 location is not linearly correlated to changes in spark timing. This leads to a close grouping of knock-limited CA50 (KLCA50) for PRFs at the knock threshold of 0.6 bar MAPO. The knockmeter knock intensity in *Figure 4B* showed less sensitivity towards changes in the flame propagation. It is noted, that the described phenomenon was only seen under stoichiometric operation, which utilized an increased compression ratio over the standard PKL operation.

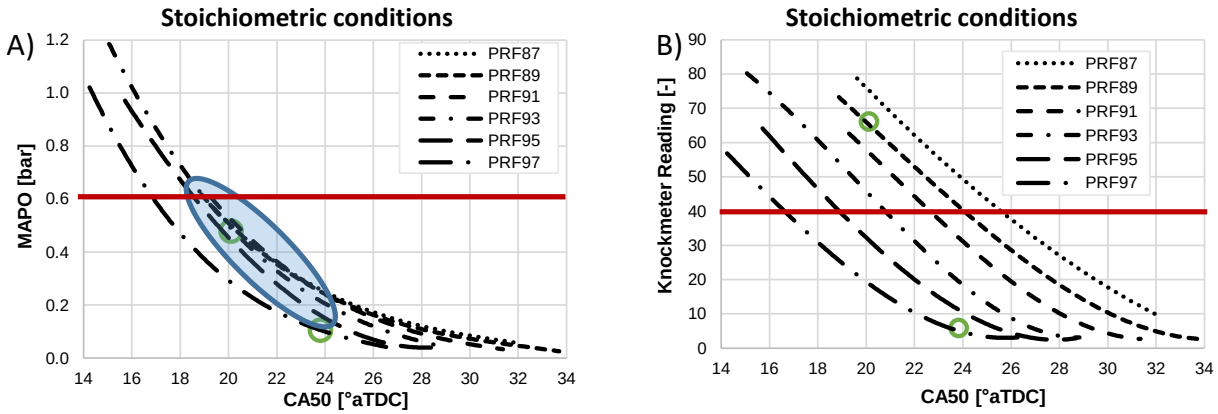

Figure 4. Knock intensity comparison for PRFs on a CA50 basis at stoichiometric conditions with a cluster of points (blue circled). The applied knock thresholds are marked as red lines.

As previously outlined, the duration between spark timing and the center of combustion (CA50) changes with the fuel. *Figure 5* shows a crank-angle resolved cylinder pressure trace and the respective rate of heat release for PRF97 (black curve) and a PRF89 (blue curve) at stoichiometric conditions. Both fuels were operated at identical spark timings and were highlighted with green circles in *Figure 3* and *Figure 4*.

The representative cycle was selected based on numerous characteristics such as pressure and location of CA50 and knockpoint, the MAPO knock intensity, the gIMEP, the maximum pressure rise rate and its location, and the cylinder pressure at spark timing [23]. Therefore, it was ensured to select a pressure trace that is most representative of each case without using an averaged trace that would average out knocking characteristics.

Figure 5A shows the full combustion event from spark timing to end of combustion as characterized by CA90. The locations of spark timing, CA50, CA90, and knockpoint are marked on the rate of heat release and on the pressure traces. The PRF89 generally showed a higher pressure trace compared to PRF97 because PRF89 had advanced combustion phasing despite being operated with an identical spark timing. The CA50 of PRF89 occurs about 3.5 CAD earlier compared to PRF97. Multiple studies discussed the knockpoint as a typical inflection point in the pressure trace due to cascading autoignition [1, 4, 8, 19]. For PRF89, the crank angle location of knockpoint was almost identical to CA50, which means that almost 50% of the charge mass auto-ignited. This led to a steep increase in the apparent heat release and a much-reduced duration from CA50 to CA90 for PRF89. The PRF97 showed slower combustion with a more delayed center of combustion and knockpoint towards the end of the combustion event. This led to a lower knock intensity compared to the PRF89 which clearly showed pressure oscillations.

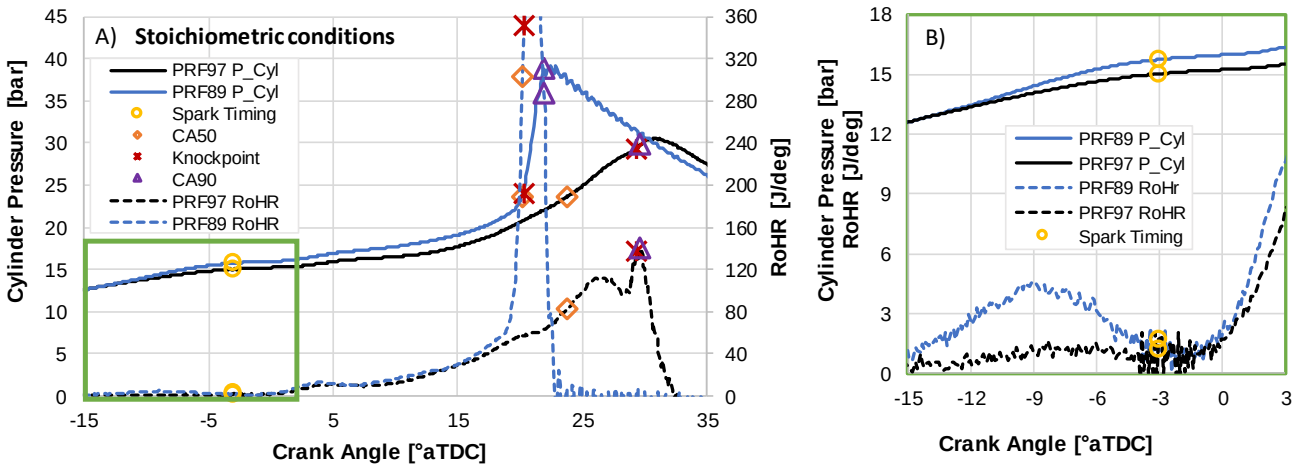

Figure 5. Crank angle resolved pressure trace and apparent rate of heat release (RoHR) for PRF89 and PRF97 at stoichiometric conditions.

Figure 5B shows a zoomed-in perspective of the green highlighted box from *Figure 5A*. The cylinder pressures for PRF97 and PRF89 closely match up to-15°aTDC but diverge before spark timing. An analysis of the apparent rate of heat release revealed a pre-spark heat release, also called low-temperature heat release (LTHR). Multiple publications recently analyzed LTHR during compression-ignition as well as spark-ignition modes [13, 21, 26, 27]. Generally, PRFs are prone to exhibit low-temperature chemistry compared to toluene or ethanol blends. Also, LTHR was noticeable in spark-ignition operation when retarding the spark timing [26]. The low-temperature heat release before spark timing caused an increased cylinder pressure for PRF89. The higher RON PRF97 did not exhibit a noticeable LTHR. Therefore, the low-temperature chemistry for PRF89 increased the flame propagation and subsequently advanced the center of combustion. For further analysis, the spark timing will be used as it was the varied parameter during the experimental study and is not affected by increased flame propagation or low-temperature heat release like CA50 would be.

3.2. FACE Fuels

Spark timing sweeps similar to *Figure 3* were performed for all fuels mentioned in *Section 2. Experimental Procedure*. *Figure 6* shows the cylinder pressure-based knock intensity MAPO, the knockmeter knock intensity, and the gIMEP as a function of spark timing for the FACE fuels and the two TSFs in comparison to the previously discussed PRFs. While wide spark timing sweeps were performed, *Figure 6* focuses on the relevant spark timings at which either of the two knock thresholds or the maximum brake torque (MBT) was achieved. The tests were performed at peak knocking lambda (*Figure 6A, C, E*), as well as at stoichiometric conditions (*Figure 6B, D, F*), which resembles modern engine operation. During experimental testing, both the knockmeter and MAPO knock intensity vary (compare [4]). Therefore, it is not possible to have an experimental data point directly at the knock threshold. Instead, for each fuel, a third-order regression polynomial was created for the MAPO and knockmeter response over a wide range of spark timings. An excellent curve fit was ensured with each coefficient of determination (R^2) exceeding 0.99.

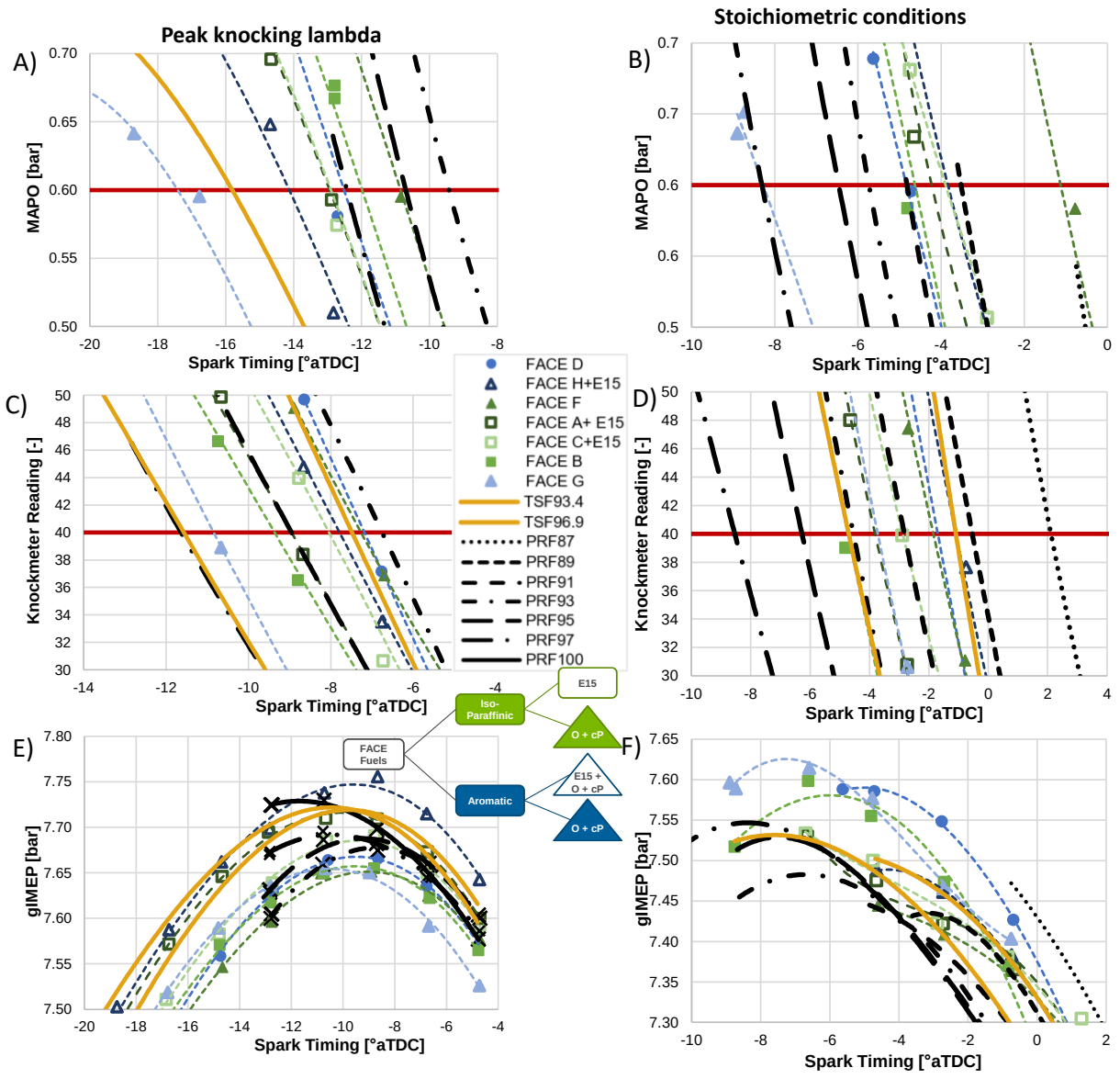

Figure 6. Spark timing sweeps at peak knock lambda conditions (A, C, E) and stoichiometric conditions (B, D, F) for MAPO knock intensity, knockmeter knock intensity, and gIMEP for all fuels.

Fuel composition-specific differences in the MAPO-based KLSA can be seen in *Figure 6A* and *Figure 6B*. Primarily paraffinic FACE fuels (green) tend towards a more retarded KLSA compared to aromatic gasolines (blue) and highly aromatic TSFs (orange). At peak knocking lambda conditions, PRF97 had a significantly retarded MAPO-based KLSA compared to highly aromatic fuels while it successfully bracketed all fuels at stoichiometric conditions. *Figure 6C* and *Figure 6D* show the knockmeter-based spark timing

sweeps at which the PRFs bracketed all sample fuels. A composition-based (aromatic vs. paraffinic) trend was not apparent. At peak knocking lambda conditions, each spark timing sweep was performed past the maximum brake torque (MBT) timing while under stoichiometric conditions, PRF87 did not reach the MBT timing. All MAPO and knockmeter-based KLSA as well as the MBT for stoichiometric conditions and PKL conditions are summarized in *Table 3*.

As can be seen from *Figure 6* and *Table 3*, the KSLA and MBT timing occur at a more advanced timing for PKL conditions compared to stoichiometric conditions. As shown in [4], the lambda of peak knock intensity is typically rich. When shifting to a stoichiometric condition, the knock intensity reduced when tested at a constant compression ratio. Under stoichiometric operation during this study, a higher compression ratio was used compared to PKL conditions which resulted in a more retarded combustion limitation under stoichiometric conditions. Under PKL conditions, the MBT timing occurred later than either KLSA timing. Therefore, the engine was not knock limited at the maximum torque output. For stoichiometric conditions, the operation at an increased compression ratio resulted in MBT timings earlier than KLSA timings. Additional spark advance beyond the knock threshold would benefit the combustion and result in increased torque output. For both PKL and stoichiometric operation, the crank angle difference between MAPO-based and knockmeter-based KLSA varied among the FACE fuels. Primary paraffinic FACE gasolines (FACE B, F, A+E15, and C+E15) show only small differences up to one crank angle degree while primary aromatic FACE gasolines typically show about two to four crank angle degrees later KLSA when based on the knockmeter. The PRFs did not always mirror this trend as it seemed dependent on the respective RON level of the PRF. The timing differences between knockmeter and MAPO-based KLSA for paraffinic and aromatic FACE fuels is due to the difference in knock intensity measurement characteristic. The MAPO is only considering pressure oscillations while the knockmeter is affected by the pressure rise rate as well [8]. Therefore, at a given MAPO knock intensity, the pressure rise rate of a chemical group of fuels can vary as shown in *Figure 7*.

Table 3. Overview of KLSA data for PKL and stoichiometric operation based on MAPO and knockmeter knock intensity.

*Legend: * extrapolated | ** MBT not reached due to knock limitation of the engine | *** Knock threshold not reached*

Fuel	Peak Knocking Lambda			Stoichiometric Conditions		
	MAPO KLSA [°aTDC]	Knockmeter KLSA [°aTDC]	Location of MBT [°aTDC]	MAPO KLSA [°aTDC]	Knockmeter KLSA [°aTDC]	Location of MBT [°aTDC]
FACE-B	-12.0	-13.3	-8.8	-4.6	-4.7	-6.6
FACE-D	-12.5	-10.2	-8.6	-4.8	-1.7	-5.2
FACE-F	-10.8	-10.7	-8.9	-1.1	-1.8	-4.6
FACE-G	-17.4	-14.3	-10.7	-8.3	-3.7	-6.6
FACE-A + E15	-12.9	-12.9	-10.7	-4.2	-3.8	-6.7
FACE-C + E15	-12.9	-11.8	-8.8	-3.9	-2.9	-6.7
FACE-H + E15	-14.1	-11.3	-8.7	-3.8	-1.1	-4.6
PRF87	Not tested	Not tested	Not tested	-1.0	+2.1	N/A**
PRF89	Not tested	Not tested	Not tested	-3.5	-0.5	N/A**
PRF91	Not tested	Not tested	Not tested	-4.8	-2.8	N/A**
PRF93	-9.8	-10.0	-8.7	-5.7	-4.5	-5.7
PRF95	-10.8	-12.4	-10.7	-6.5	-6.3	-8.7
PRF97	-12.4	-15.4	-10.7	-8.3	-8.5	-8.7
PRF100	-17.3 *	-18.5	-10.7	Not tested	Not tested	Not tested
TSF93.4	-15.8	-10.6	-10.7	-6.4	-1.1	N/A**
TSF96.9	N/A***	-15.5	-10.7	-10.3	-4.7	-8.8

As previously mentioned, the pressure-based knock intensity threshold was selected to 0.6 bar, representing 1 bar cylinder pressure oscillations per 1000 rpm. For stoichiometric operation, *Figure 7* correlates the 300 cycle-averaged MAPO and the maximum pressure rise rate for the spark timing sweeps of the FACE fuels, PRFs, and TSFs. Advanced spark timing led to both a higher MAPO knock intensity as well as maximum pressure rise rate. A clear distinction between mainly paraffinic (green) and primarily aromatic (blue) fuels can be observed. Highly paraffinic fuels showed a much reduced maximum pressure rise rate which supports the previously discussed smaller crank angle degree difference between knockmeter- and MAPO-based KLSA for *Figure 6* and *Table 3*. Similarly, the PRFs and TSFs support the clear distinction between primarily paraffinic and aromatic fuels based on their difference in maximum pressure rise rate at a given MAPO knock intensity.

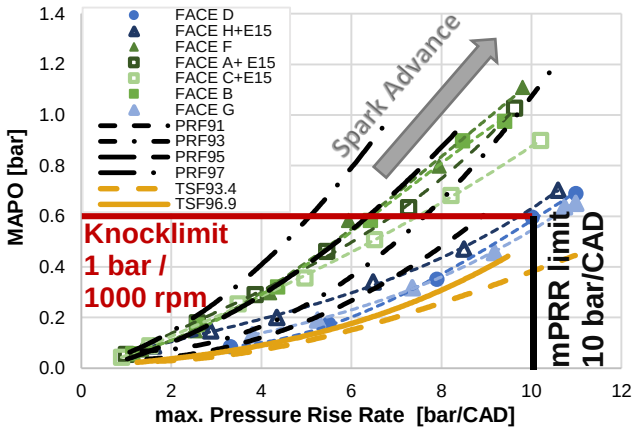

Figure 7. Correlation between the maximum amplitude of pressure oscillations (MAPO) and the maximum pressure rise rate (mPRR) at stoichiometric conditions with defined operation thresholds.

For further analysis, only the MAPO knock intensity limit was applied and the maximum pressure rise rate limit was neglected to ensure all fuels would be rated based on a common characteristic. It was also found that a reduced MAPO threshold resulted in an identical order of fuels while not reaching the maximum pressure rise rate threshold.

4. KLSA-based Octane Correlations

Knock assessment in modern engines as characterized by the knock limited spark advance (KLSA) based on a pressure-based knock intensity threshold is widely common but its correlation to the standard RON rating of the fuel is often inadequate [5, 6, 13, 20]. *Figure 8* shows the KLSA of FACE fuels, PRFs, and TSFs under PKL (*Figure 8A* and *Figure 8B*) and stoichiometric (*Figure 8C* and *Figure 8D*) conditions compared to the standard RON rating of the fuels. The previous publication showed significant differences in the knock intensity response for lambda sweeps which will impact the KLSA ratings between the two conditions [4]. For both PKL and stoichiometric operation, the knock threshold was based on either 0.6 bar maximum amplitude of pressure oscillations (*Figure 8B, D*) or a knockmeter reading of 40 KU (*Figure 8A, C*). For each plot within *Figure 8*, a linear trendline for all fuels along with its coefficient of determination (R^2) is shown to quantitatively evaluate the correlation. Across all plots, increased RON generally allowed for more spark advance but important discrepancies between fuels were observed.

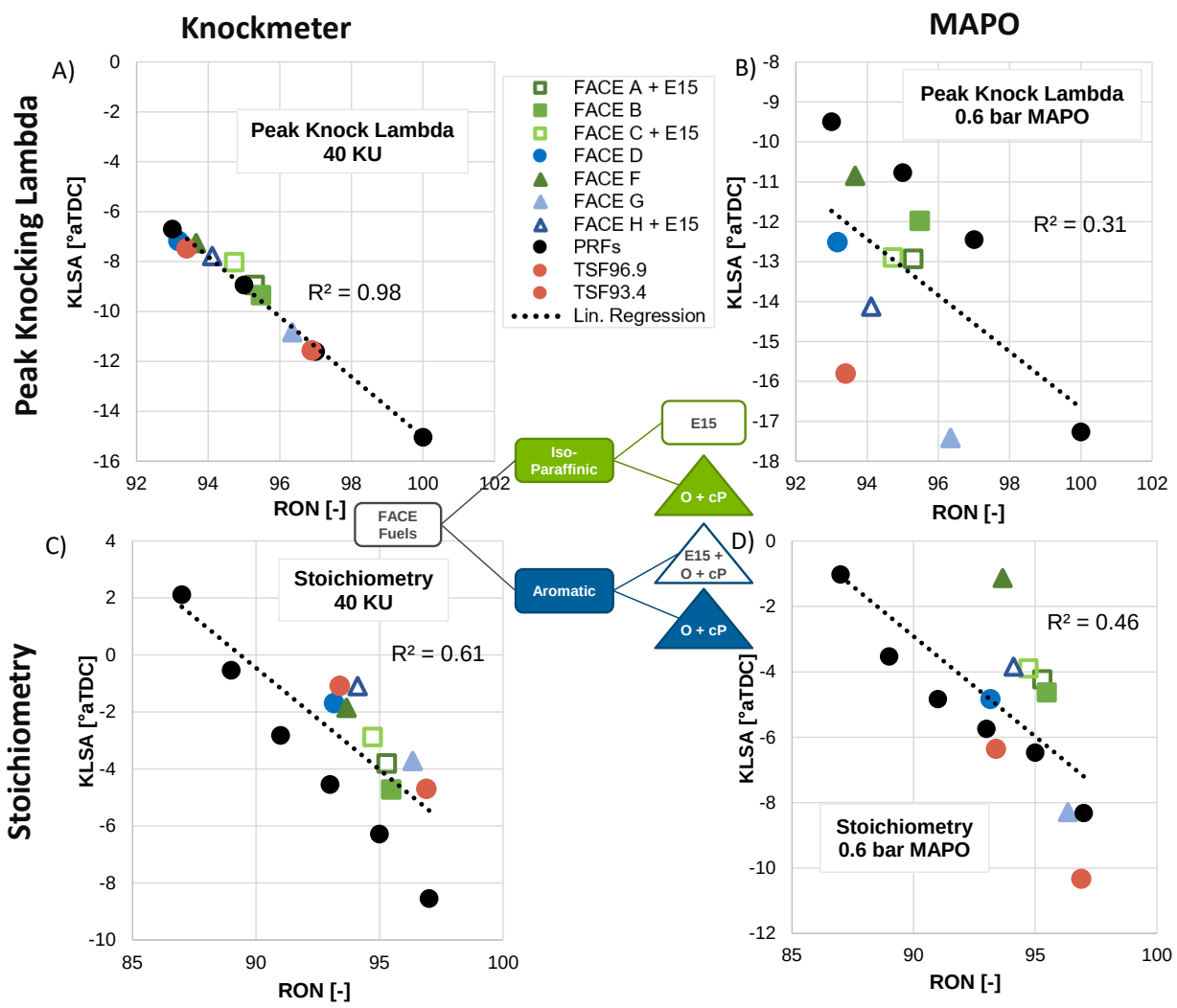

Figure 8. Correlations between the knock limited spark advance (KLSA) and standard RON ratings for varying operating conditions.

An excellent correlation was found between the knockmeter-based KLSA at PKL operation and RON, *Figure 8A*. This can be explained by the similarity between the testing conditions and the standard RON test which both use the same air-to-fuel ratio as well as knock intensity characterization method. Only the spark timing and hence the knock intensity differ. Generally, the KLSA showed better correlations when based on the knockmeter compared to MAPO. When keeping PKL operation but using a MAPO threshold, the correlation significantly reduced to R^2 = 0.3, *Figure 8B*. This poor correlation followed previous findings of the first publication, where the MAPO knock intensity during a standard RON rating did not

correlate to the fuel's RON rating [4]. As a result, the KLSA for the fuels also varies significantly. The PRFs previously showed the highest MAPO ratings and hence required the most retarded spark timings at PKL conditions. Furthermore, primarily paraffinic FACE fuels (green markers) showed the second most retarded KLSAs which aligns with the slightly reduced MAPO ratings in the first publication [4]. Predominantly aromatic FACE fuels (blue markers) and mostly aromatic TSFs (orange markers) tended towards the most advanced KLSAs following their previously described lower MAPO ratings under standard RON conditions.

When shifting operation from PKL (*Figure 8A*) to stoichiometric (*Figure 8C*), the correlation between knockmeter and RON reduced significantly due to the larger deviation from the standard RON test. The PRFs showed the most advanced KLSA while all falling on a separate imaginary trendline. The advanced KLSA of PRFs in *Figure 8C* is contradicting the most retarded KLSA of PRFs in *Figure 8B*. This can be explained by the different methods of evaluating knock intensity. Among a common knockmeter reading, the MAPO reading changes significantly with fuel composition. Furthermore, as shown in the previous study, the lambda dependence of knock intensity needs consideration as the lambda of peak knock intensity for PRFs was the richest at approximately $\lambda = 0.88 – 0.89$ [4]. Subsequently, the PRFs underwent the largest lambda change when switching from PKL to stoichiometric which resulted in the largest effect on knock intensity. This hypothesis was confirmed by FACE-B, which had the second richest PKL in the previous study and now showed a slightly advanced KLSA amongst the FACE fuels in *Figure 8C* [4]. Furthermore, FACE-H+E15 and FACE-G show the most retarded KLSA in *Figure 8C* while having the closest to stoichiometric peak knocking lambda in the previous study [4]. For stoichiometric operation, the MAPO-based KLSA correlation to RON in *Figure 8D* is poor but slightly improved upon MAPO-based PKL operation in *Figure 8B*. The authors previously showed that a MAPO-based RON at stoichiometric conditions somewhat correlated to the standard RON ratings amongst the FACE fuels [4]. *Figure 8D* shows the FACE fuels grouped by their chemical composition. In contrast, the PRFs fall on a separate imaginary

trendline which reduced the overall correlation. Of the FACE fuels, the mainly paraffinic blends (green markers) showed a more retarded KLSA compared to the aromatic fuels (blue markers). This was in line with findings from the previous study by the authors which showed that the effective MAPO-based RON at stoichiometric conditions for aromatic fuels was close to the standard RON rating while that of primarily paraffinic FACE fuels had a lower effective MAPO-based RON at stoichiometric conditions than their standard RON rating [4]. This translates to the KLSA grouping of aromatic and paraffinic FACE fuels in *Figure 8D*. It is also noted that the TSFs showed the most advanced KLSA while having the highest concentration of aromatic components.

Figure 8 compared the KLSAs for all fuels to their standard RON with correlations ranging from very good (R^2 = 0.98) in the case of a knockmeter-based PKL operation to poor (R^2 = 0.31) for MAPO-based PKL operation. Literature shows Octane Index to better correlate to modern engine operation which includes the use of a cylinder pressure-based knock intensity like MAPO. *Figure 9* shows the identical KLSA data from *Figure 8* but compares it to Octane Index, which was calculated using equation 1 and the standard RON and MON values of the fuels. Each correlation was optimized for the highest coefficient of determination (R^2) by altering the engine operation-specific K-factor. Both coefficients are shown on each plot in *Figure 9*.

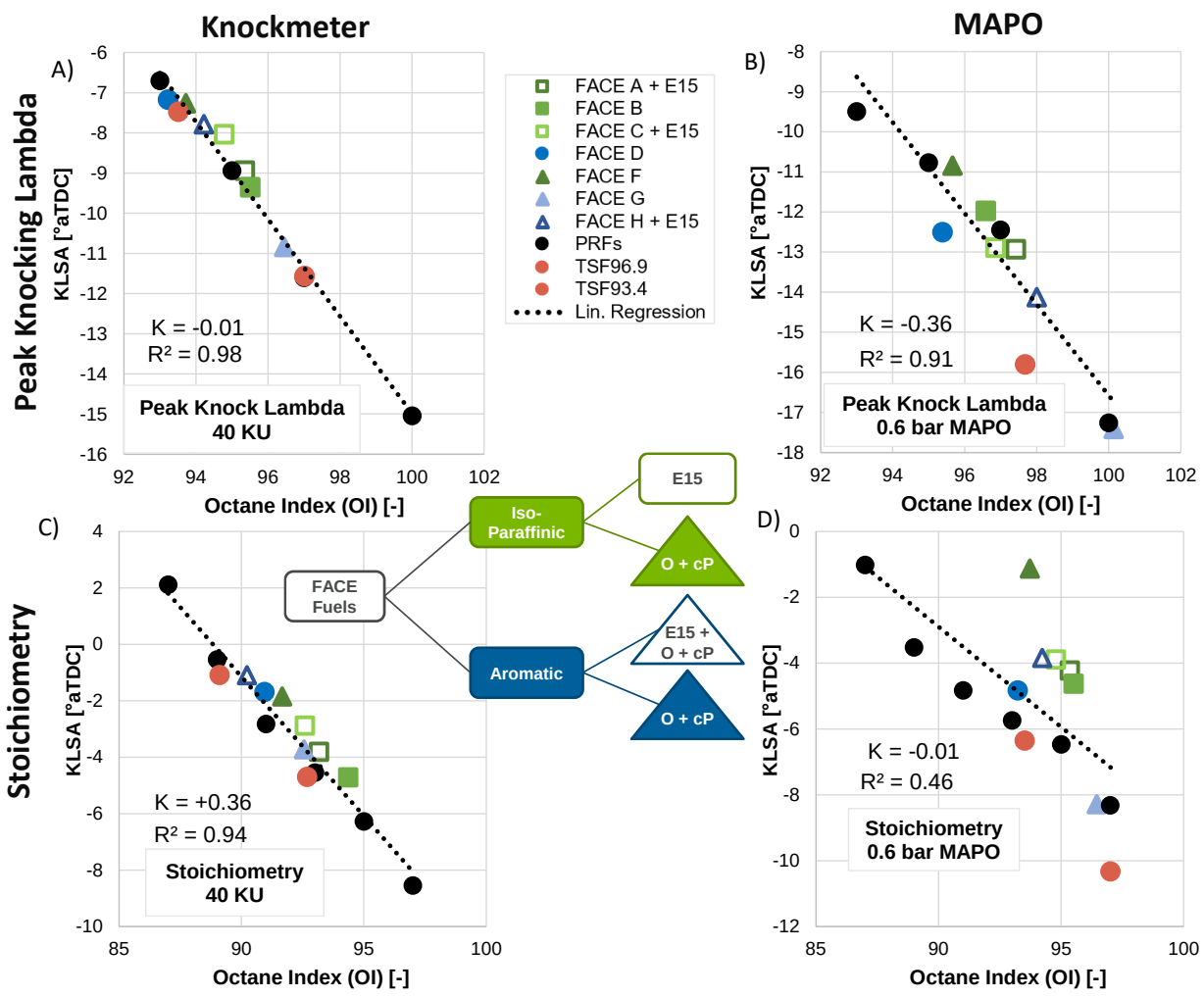

Figure 9. Correlations between the knock limited spark advance (KLSA) and Octane Index for varying operating conditions with K optimized for the best correlation.

The KLSA for the knockmeter threshold under PKL operation already strongly correlated to the RON ratings of the fuels in *Figure 8*. This was no surprise and was due to the similarity to the standard RON test as it only deviated in terms of knock threshold and spark timing. The introduction of Octane Index did not further improve the coefficient of determination and the engine operation-specific factor K is essentially zero, *Figure 9A*. Switching to a MAPO-based knock threshold at PKL conditions, KLSA showed the worst correlation to RON in *Figure 8B*. This is in line with findings from the first part of this three-part publication series where MAPO under standard RON conditions did not correlate to the fuel's standard RON rating

[4]. The first part showed mainly paraffinic fuels with increased MAPO knock intensities under standard RON conditions compared to aromatic fuels which resulted in a more retarded KSLA in *Figure 8* [4]. Switching to Octane Index significantly improved the correlation to KLSA but required a K-factor of K = -0.36, *Figure 9B.* This again is very similar to the findings from the first part which showed the best correlation between MAPO and Octane Index at K = -0.48 [4]. A negative K-factor effectively means engine operation at beyond RON conditions while the engine mostly operates under RON conditions except for the knock threshold and spark timing. Knock limited spark advance studies in the literature typically associate K = 0 with RON conditions but this study suggests a slightly negative K-factor would yield a better comparison when using a MAPO-based knock threshold. Moving towards stoichiometric conditions and using a knockmeter-based threshold, the KLSA correlation to Octane Index greatly improved compared to standard RON, *Figure 8C* and *Figure 9C*. While the knockmeter was largely affected by the gap between PKL and stoichiometric, Octane Index counteracted that effect and yielded an excellent correlation. It is noted that the K = +0.36 showed a distinct move towards the fuel's antiknock index (K = 0.5). Furthermore, the combined findings from *Figure 8C* and *Figure 9C* suggest that the lambda of peak knock and the RON-MON sensitivity could be linked since the RON-MON sensitivity and the PKL mostly moved coherently. While MON testing is not part of this three-part series, it is noted that literature shows a generally closer to stoichiometric PKL under MON conditions [28]. When operating the engine with a MAPO-based threshold at stoichiometric conditions, which best resembles modern engine testing, no benefit of Octane Index over RON was found and the coefficient of determination remained low with a K-factor of around zero, *Figure 8C* and *Figure 9D*. This disappointing correlation with some recognizable trend with RON and Octane Index is in line with literature which shows an improvable correlation between RON and KLSA data tested on modern SI research engines [8, 13, 20]. It is also noted that varying the knock threshold outside of 0.6 bar MAPO or 40 knockunits affected the KLSA accordingly but the correlations from *Figure 8* and *Figure 9*, as well as the K-factor optimizations, remained largely similar.

The standard octane test rates the knock intensity of a sample fuel relative to that of PRFs. Applying a similar methodology, the measured KLSA values of the sample fuels are normalized by the KLSAs of respective PRFs. Subsequently, an effective octane number based on KLSA was calculated using interpolation between the applicable PRFs. *Table 4* shows the effective octane numbers for the knockmeter- and MAPO-based KLSA values on the basis of KLSA values from *Table 3*. For comparison, *Table 4* also shows the standard RON of each fuel. The calculations were performed for stoichiometric conditions as well as each fuel under its individual peak knocking lambda operation. While most KLSA-based effective RONs were interpolated, some fuels had their KLSA value outside of the boundaries set by the PRFs and required extrapolation. The correlation between the calculated effective KLSA-based RONs to the standard RON would follow the trends shown in and described for *Figure 8*.

The additional value of the effective RON calculations is the order of sample fuels relative to PRFs. For FACE fuels and TSFs, the effective knockmeter KLSA-based RON at PKL is within 0.8 octane of their standard RON with is only slightly outside the 0.7 RON reproducibility of the standard RON test. Using a MAPO-based knock intensity evaluation under PKL conditions, the effective RON of the FACE fuels and TSFs increased in comparison to their standard RON suggesting that they had a retarded KLSA compared to PRFs. On the contrary, the MAPO-based RON under stoichiometry significantly reduced the effective RON compared to both standard RON and PKL MAPO RON for most of the sample fuels with the exception of FACE-G and both TSFs. These are the fuels with the highest RON-MON sensitivity as well as the highest aromatic content.

Table 4. Overview of KLSA-based RON values for PKL and stoichiometric operation based on MAPO (0.6 bar) and knockmeter (40 KU) knock intensity.

*Legend: * extrapolated | ** RON defined based on volumetric iso-octane content | *** did not reach the knock threshold*

Fuel	Standard RON	Peak Knocking Lambda		Stoichiometric	
		MAPO KLSA-based RON [-]	Knockmeter KLSA-based RON [-]	MAPO KLSA-based RON [-]	Knockmeter KLSA-based RON [-]
FACE-B	95.8	96.4	95.3	90.7	93.2
FACE-D	94.2	97.1	93.4	91.0	90.0
FACE-F	94.0	95.1	93.5	87.1	90.1
FACE-G	96.5	100.1*	96.4	97.0	92.0
FACE-A + E15	94.8	97.6	95.0	90.1	92.1
FACE-C + E15	94.8	97.5	94.2	89.6	91.1
FACE-H + E15	94.1	98.0	94.0	89.5	89.5
PRF87**	87	Not tested	Not tested	87	87
PRF89**	89	Not tested	Not tested	89	89
PRF91**	91	Not tested	Not tested	91	91
PRF93**	93	93	93	93	93
PRF95**	95	95	95	95	95
PRF97**	97	97	97	97	97
PRF100**	100	100	100	Not tested	Not tested
TSF93.4	93.4	99.1	93.7	94.7	89.5
TSF96.9	96.9	N/A***	97.0	99.2*	93.2

The KLSA-based effective RON ratings from *Table 4* under stoichiometric operation using a MAPO knock intensity threshold best represent how modern commercial engines perform knock testing but *Figure 8* showed a poor correlation to its standard RON while switching to Octane Index in *Figure 9* also did not improve upon it. *Figure 10* shows a comparison of the effective KLSA-based RON rating from this study to the MAPO-based effective RON from the previous work [4]. Both tests were conducted using a MAPObased knock intensity under stoichiometric conditions. Only fuels that were common between both test sets are displayed. The PRFs have a defined effective RON rating based on their volumetric concentration of iso-octane. Subsequently, they are expected to exactly line up. The overall correlation as quantitively expressed by the coefficient of determination is acceptable. Except for FACE-G, all FACE fuels showed a higher MAPO-based RON. The difference between the two datasets is in the spark timing and the level of knock intensity. Most of the FACE fuels showed a slight reduction in relative knock resistance when tested under KLSA conditions which could result from the retarded spark timing or the reduced level of knock intensity or a combined effect of both parameters. Subsequently, the third study of this publication series will combine these findings and maintain constant combustion phasing as well as a constant knock intensity by varying the compression ratio.

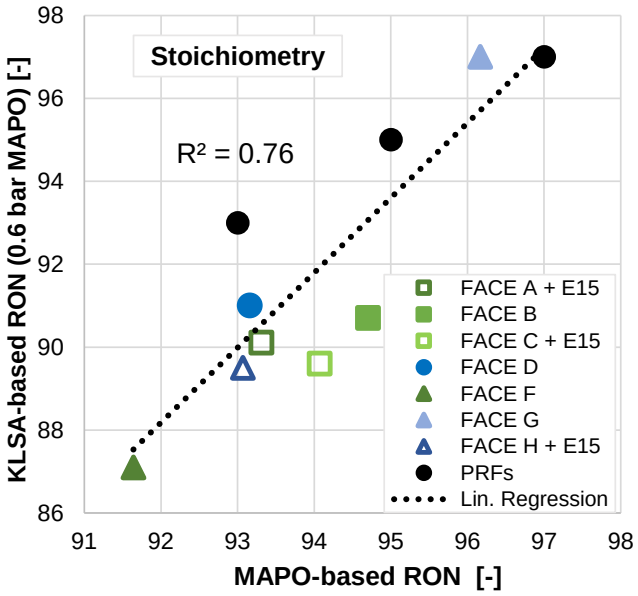

Figure 10. Comparison of the KLSA-based effective RON results with the MAPO-based effective RON from the previous work [4].

5. Summary

The observations of this work can be summarized as follows:

- Knock-limited spark advance sweeps were performed for FACE and reference fuels on the standard octane rating CFR engine under peak knocking lambda and stoichiometric operation for a knockmeter- and a maximum amplitude of pressure oscillation-based (MAPO) knock intensity threshold.
- The use of knock-limited spark advance (KLSA) proved superior compared to the knock-limited combustion phasing (KLCA50). A detailed heat release analysis found autoignition to occur simultaneously to the center of combustion which caused undesirable effects on KLCA50. Low-temperature heat release before spark timing occurred for low RON PRFs at retarded spark timings.

- Primarily paraffinic fuels tended towards higher pressure oscillations while fuels with increased aromatic content showed higher pressure rise rates.
- A knockmeter-based KLSA under PKL conditions showed the best correlation to RON due to its similarity to the standard RON test. Using a MAPO-based knock intensity threshold under PKL conditions resulted in a poor correlation to RON. Shifting from RON to Octane Index significantly improved the correlation to an excellent fit but at a K-factor of K = -0.36 which resembles RON-like KLSA testing on modern engine platforms. A MAPO-based stoichiometric KLSA similar to modern engine knock testing had a poor correlation to RON while Octane Index only slightly improved the correlation which validates the limited applicability of RON in modern engine operation.
- The KLSA-based stoichiometric RON using a MAPO knock intensity threshold correlated reasonably well with the MAPO-based stoichiometric RON from the first part of this publication series. All but FACE-G showed an offset towards increased MAPO-based RON.

This study applied the methods of modern engine knock characterization to the standard octane rating CFR engine. A MAPO-based KLSA rating under stoichiometry showed only a poor correlation to RON or Octane Index. A better correlation was found between the KLSA-based stoichiometric RON and the MAPO-based stoichiometric RON from the first study of this three-part publication series. However, except for FACE-G, all FACE fuels showed slightly increased MAPO-based RON results. Since both the knock intensity and the spark timing varied simultaneously, a final answer to the cause of this offset is targeted for the third study. The interlinked parameters combustion phasing and knock intensity will be kept constant by varying the compression ratio.

6. Acknowledgments

The authors would like to thank the Coordinating Research Council (CRC) task group Advanced Vehicle Fuel Lubricants AVFL-32 for providing the FACE fuels, funding, and project guidance.

The authors would also like to acknowledge the support and contribution of Dr. Scott Miers, thank Dr. Stephan Schneider for his assistance during the experimental work, and thank Timothy Rutter for his technical support.

Argonne is a U.S. Department of Energy laboratory managed by UChicago Argonne, LLC under contract DE-AC02-06CH11357.

7. References

1. Swarts, A. and Yates, A., "Insights into the Role of Autoignition during Octane Rating," SAE Technical Paper 2007-01-0008, 2007, doi.org/10.4271/2007-01-0008.
2. ASTM D2699-15a, “Standard Test Method for Research Octane Number of Spark-Ignition Engine Fuel,” ASTM International, West Conshohocken, PA, 2015, doi: 10.1520/D2699-15A
3. ASTM D2700-16, “ Standard Test Method for Motor Octane Number of Spark-Ignition Engine Fuel,” ASTM International, West Conshohocken, PA, 2016, doi: 10.1520/D2400-16
4. Hoth, A., Kolodziej, C., “Effects of knock intensity measurement technique and fuel chemical composition on the research octane number (RON) of FACE gasolines: Part 1 – Lambda and

knock characterization", Fuel, Volume 304, 2021, 120722,ISSN 0016-2361, https://doi.org/10.1016/j.fuel.2021.120722.

5. Swarts, A., Yates, A., Viljoen, C., and Coetzer, R., "A Further Study of Inconsistencies between Autoignition and Knock Intensity in the CFR Octane Rating Engine," SAE Technical Paper 2005-01-2081, 2005, doi:10.4271/2005-01-2081.

6. Swarts, A., Anderson, G., and Wallace, J., "Comparing Knock between the CFR Engine and a Single Cylinder Research Engine," SAE Technical Paper 2019-01-2156, 2019.

7. Huber, K., Hauber, J., Raba, A., and Nell, R., "New Test Procedure to Determine Fuel's Knock Resistance," MTZ-Motortechnische Zeitschrift 74(7/8):62-69, 2013.

8. Rockstroh, T., Kolodziej, C., Jespersen, M., et al., "Insights into Engine Knock: Comparison of Knock Metrics across Ranges of Intake Temperature and Pressure in the CFR Engine," SAE Technical Paper 2018-01-0210, 2018, doi:10.4271/2018-01-0210.

9. Heywood, J., "Internal Combustion Engine Fundamentals," New York: McGraw-Hill, 1998. ISBN: 0-07-028637-X

10. Hoth, A., Kolodziej, C., Rockstroh, T. et al., "Combustion Characteristics of Match-Blended PRF and TSF Fuels with Ethanol in an Instrumented CFR Engine," SAE Technical Paper 2018-01-1672.

11. Hauber, J., Huber, K., and Nell, R., "New GKI - Gasoline Knock Index for Rating of Fuel's Knock Resistance on an Upgraded CFR Test Engine," SAE Technical Paper 2018-01-1743, 2018.

12. Hoth, A., Pulpeiro Gonzalez, J., Kolodziej, C., and Rockstroh, T., "Effects of Lambda on Knocking Characteristics and RON Rating," SAE Int. J. Adv. & Curr. Prac. in Mobility 1(3):1188-1201, 2019, https://doi.org/10.4271/2019-01-0627.

13. J. Szybist, D. Splitter, "Understanding chemistry-specific fuel differences at a constant RON in a boosted SI engine", Fuel, Volume 217, 2018, Pages 370-381, doi:10.1016/j.fuel.2017.12.100.

14. Yates, A., Swarts, A., and Viljoen, C., "Correlating Auto-Ignition Delays And Knock-Limited Spark-Advance Data For Different Types Of Fuel," SAE Technical Paper 2005-01-2083, 2005, doi:10.4271/2005-01-2083.

15. Kalghatgi, G., "Fuel Anti-Knock Quality - Part I. Engine Studies," SAE Technical Paper 2001-01-3584, 2001, doi:10.4271/2001-01-3584.

16. Morgan, N., Smallbone, A., Bhave, A., et al., “Mapping surrogate gasoline compositions into RON/MON space”, Combustion and Flame, Volume 157, Issue 6, 2010, Pages 1122-1131, https://doi.org/10.1016/j.combustflame.2010.02.003.

17. Mittal, V. and Heywood, J., "The Shift in Relevance of Fuel RON and MON to Knock Onset in Modern SI Engines Over the Last 70 Years," SAE Int. J. Engines 2(2):1-10, 2010, doi:10.4271/2009-01-2622.

18. Kolodziej, C., Pamminger, M., Sevik, J., Wallner, T. et al., "Effects of Fuel Laminar Flame Speed Compared to Engine Tumble Ratio, Ignition Energy, and Injection Strategy on Lean and EGR Dilute Spark Ignition Combustion," *SAE Int. J. Fuels Lubr.* 10(1):82-94, 2017, https://doi.org/10.4271/2017-01-0671.

19. Pulpeiro Gonzalez, J., Shah, A., Hoth, A., Rockstroh, T. et al., "Statistical Analysis of Fuel Effects on Cylinder Conditions Leading to End-Gas Autoignition in SI Engines," SAE Technical Paper 2019-01-0630, 2019, https://doi.org/10.4271/2019-01-0630.

20. Vuilleumier, D., Kim, N., Sjöberg, M., Yokoo, N. et al., "Effects of EGR Constituents and Fuel Composition on DISI Engine Knock: An Experimental and Modeling Study," SAE Technical Paper 2018-01-1677, 2018, doi:10.4271/2018-01-1677.

21. Waqas, M., Hoth, A., Kolodziej, C., Rockstroh, T. et al., "Characterization of Low Temperature Reactions in the Standard Cooperative Fuel Research (CFR) Engine," *SAE Int. J. Engines* 12(5):597-610, 2019, https://doi.org/10.4271/03-12-05-0038.

22. Cannella, W., Foster, M., Gunter, G., et al., “FACE Gasolines and Blends with Ethanol: Detailed Characterization of Physical and Chemical Properties”, CRC Report No. AVFL-24, 2014.

23. Pulpeiro Gonzalez, J., Hall, C., Kolodziej, C., “Determination of a most representative cycle from cylinder pressure ensembles via statistical method using distribution skewness”, International Journal of Engine Research, 2021. https://doi.org/10.1177/14680874211065525.

24. Lavoie, G., Ortiz-Soto, E., Babajimopoulos, A., et al., “Thermodynamic sweet spot for high-eficiency, dilute, boosted gasoline engines”, International Journal of Engine Research, Vol 14, Issue 3, 2013. https://doi.org/10.1177%2F1468087412455372

25. AVL Group, “Pressure Sensors For Combustion Analysis”, Product Catalog, 01/2013.

26. Waqas, M., Hoth, A., Kolodziej, C., et al., “Detection of low temperature heat release (LTHR) in the standard Cooperative Fuel Research (CFR) engine in both SI and HCCI combustion modes”, Fuel, Volume 256, 2019, https://doi.org/10.1016/j.fuel.2019.115745.

27. Waqas, M., Cheng, S., Goldsborough, S., et al., “An experimental and numerical investigation to characterize the low-temperature heat release in stoichiometric and lean combustion”, Proceedings of the Combustion Institute, Volume 38, Issue 4, 2021, Pages 5673-5683, https://doi.org/10.1016/j.proci.2020.07.146.

28. Morganti, K., Foong, T., Brear, M., Da Silva, G. et al., "Design and Analysis of a Modified CFR Engine for the Octane Rating of Liquefied Petroleum Gases (LPG)," *SAE Int. J. Fuels Lubr.* 7(1):283-300, 2014, https://doi.org/10.4271/2014-01-1474.

8. Abbreviations

CA50	50% Mass Fraction Burned
CA90	90% Mass Fraction Burned
CFR	Cooperative Fuel Research
CRC	Coordinating Research Council
FACE	Fuels for Advanced Combustion Engines
gIMEP	Gross Indicated Mean Effective Pressure
KLCA50	Knock Limited Combustion Phasing
KLSA	Knock Limited Spark Advance
KU	Knock Units
MAPO	Maximum Amplitude of Pressure Oscillations
MBT	Maximum Brake Torque
MON	Motor Octane Number
OI	Octane Index
PRF	Primary Reference Fuel
RON	Research Octane Number
TSF	Toluene Standardization Fuel

9. Appendix

Table 5. Combustion research measurement and instrumentation systems employed on the Argonne CFR engine.

Crankshaft angle-based measurements	
Crank-angle based DAQ	AVL IndiMicro & crankshaft encoder
Spark timing	Current clamp on coil wire
Intake pressure	Flush-mounted Kulite ETL-189-190M-2.5bara (0.2 crank-angle resolution)
Exhaust pressure	Flush-mounted Kulite EWCTV-312M-3.5bara (0.2 crank-angle resolution)
Cylinder pressure	AVL GU13Z-24 flush-mounted spark plug pressure transducer (0.1 crank angle resolution)
Time-based measurements	
Time-based DAQ	LabVIEW
Intake pressure	Setra 3550 pressure transducer
Exhaust pressure	Setra 3550 pressure transducer
Intake, mixture, exhaust, coolant, and oil temperature	K-type thermocouples
Fuel rate	Emerson CMF010M Coriolis Meter
Lambda	Bosch wide-band lambda sensor LSU 4.9
CFR knock units	Data-logged knockmeter signal